ISTITUTO NAZIONALE DI FISICA NUCLEARE

Sezione di Milano

INFN/AE-94/20
20 Settembre 1994

G. Bellini:

STUDY OF CHARMED MESON STATES PHOTOPRODUCED AT HIGH ENERGY AT FERMILAB

PACS.: 14.20.Kp, 13.30.Eg/AE

Paper submitted to the ICHEP '94

Servizio Documentazione
dei Laboratori Nazionali di Frascati

INFN - Istituto Nazionale di Fisica Nucleare
Sezione di Milano

INFN/AE-94/20
20 Settembre 1994

STUDY OF CHARMED MESON STATES PHOTOPRODUCED AT HIGH ENERGY AT FERMILAB

G. Bellini
Dipartimento di Fisica dell'Universita' - Milano
Istituto Nazionale di Fisica Nucleare - Milano
on behalf of the E687 Collaboration*

ABSTRACT

The E687 Collaboration has obtained further results on the charmed mesons. In this paper we report: some results on the correlations in the production mechanisms, new measurements of the lifetime, studies of decay channels Cabibbo suppressed or going via annihilation or exchange diagrams, analysis of substructures, measurements of the form factors in the semileptonic channels, limits on CP violation.

1. Introduction

The E687 experiment collected about 10^5 charmed particles at a photon beam with 220 GeV mean energy at Fermilab. The detector, described elsewhere[1], is a large aperture multiparticle spectrometer with good detection capabilities for charged hadrons and photons. The tracking system includes a microvertex detector (twelve planes of silicon microstrip detectors: $\sigma_\tau \approx 0.04\ ps$), two magnets and 5 MWPC stations with 4 views. Three $\check{C}$ counters, ~100 cell each, allow a good particle identification (kaon identification from 5 to 62 GeV). Finally two fine grain em calorimeters (large Ω), one hadron calorimeter, two muon detectors (inner and outer) are installed.

In this paper I will discuss some of the more recent results achieved by the collaboration on the charmed mesons.

---

* P.L. Frabetti (Bologna), G.P. Grim, V.S. Paolone, P.M. Yager (Davis), H.W.K. Cheung, J.P. Cumalat, C. Dallapiccola, J.F. Ginkel, S.V. Greene, W.E. Johns, M.S. Nehring (Colorado), J.N. Butler, S. Cihangir, I. Gaines, P.H. Garbincius, L. Garren, S. Gourlay, D.J. Harding, P. Kasper, A. Kreymer, P. Lebrun, S. Shukla (Fermilab), S. Bianco, F.L. Fabbri, S. Sarwar, A. Zallo (Frascati), R. Culbertson, R.W. Gardner, R. Greene, J. Wiss (Illinois), G. Alimonti, G. Bellini, B. Caccianiga, L. Cinquini, M. di Corato, M. Giammarchi, P. Inzani, F, Leveraro, S. Malvezzi, D. Menasce, E. Meroni, L. Moroni, D. Pedrini, L. Perasso, A. Sala, S. Sala, D. Torretta, M. Vittone (Milano), F. Davenport (North Carolina), J.F. Filasetta (Northern Kentucky), D. Buchholz, D. Claes, B. Gobbi, B. O'Reilly (Northwestern), J.M. Bishop, N.M. Cason, C.J. Kennedy, G.N. Kim, T.F. Lin, D.L. Puseljic, R.C. Ruchti, W.D. Shepard, J.A. Swiatek, Z.Y. Wu (Notre Dame), V. Arena, G. Boca, C. Castoldi, G. Gianini, S.P. Ratti, C. Riccardi, P. Vitulo (Pavia), A. Lopez (Puerto Rico), J.R. Wilson (South Carolina), G.R. Blackett, M. Pisharody, T. Handler (Tennessee), P.D. Sheldon (Vanderbilt), B.G. Cheon, J.S. Kang, K.Y. Kim (Korea).

2. Production mechanisms

E687 selected 325 ± 23 double tag events, with D and $\overline{D}$ fully reconstructed. Golden D decay modes: $K^-\pi^+\pi^+, K^-\pi^+, K^-\pi^+\pi^+\pi^-$, together with their charged conjugates, have been considered.

The main selection cut is the detachment, which requires that the decay light distance, normalized to its error, will be larger than a value up to 7, depending on the candidate topology (f.i. the detachment requirement was less restrictive for the D^* constrained events). The background was subtracted by averaging sidebands 4σ-8σ from the nominal D mass value.

We discuss here two important parameters: the transverse momentum-squared distribution of the $D\overline{D}$ pair $[P_t^2(D\overline{D})]$ and the acoplanarity angle between the D and $\overline{D}$ momentum vector in the plane transverse to the photon direction. The spectrometer acceptance and the resolution effects are very small for both these variables.

A comparison of these distributions with a Monte Carlo based upon the Lund model (gluon p_t is a gaussian with a RMS width of 0.44 GeV/c), shows disagreement for both. The $p_t^2(D\overline{D})$ experimental distribution is significantly harder than the prediction, while $\Delta\phi$ data tend to be more smeared from $\Delta\phi = \pi$ radians than the Lund expectation(2).

More recently these data have been compared with the NLO photon-gluon fusion approximation(3). It is possible to introduce in these calculations also a gluon p_t kick different from zero. The comparison is done in Figs. 1, 2.

There is a general good agreement between data and theory. The assumption of a gluon p_t kick, $<p_t^2> = 0.5\ (GeV/c)^2$, does not introduce relevant changements with respect to the NLO approximation; nevertheless the agreement between data and theoretical expectations seems improved by a small gluon p_t kick assumption.

It is important to note that the NLO approximation with a $<p_t^2>$ kick of 0.5 $(GeV/c)^2$ gives a good agreement also with the WA92 hadroproduced results(3,4) (see Fig. 3).

In all the NLO calculations shown in Figs. 1,2,3, the renormalization scale μ is defined=M_C and M_C is assumed = 1.5 GeV, which is a very reasonable value.

3. Lifetime measurements

New lifetime measurements have been obtained by E687 with a very carefull study of the systematic effects.

The measurement of the charmed meson lifetime has been made using the following decay modes:

$D^\pm \to K^-\pi^+\pi^+$, $D^0 \to K^-\pi^+$, $D^0 \to K^-\pi^+\pi^-\pi^+$ (NOTAG sample), $D^{*\pm} \to \pi^\pm D^0$ (TAG sample), $D_s^\pm \to \phi\pi^\pm$.

3.1 Selection of the samples

In selecting the charm signal, the effects of the detachment cuts have been studied from $\ell/\sigma_\ell > 0$ to $\ell/\sigma_\ell > 20$. The secondary vertex was required to be upstream of the first trigger counter

in order to reduce systematic effects due to charmed particles decaying very close to or within the microstrip detector.

For the neutral D, the D^* tag events were identified by looking for a pion of correct charge, which could be combined with the reconstructed D^0 such that $M(\pi^+D^0)-M(D^0)$ lies within 2 MeV of the world average $D^{*+}-D^0$ mass difference.

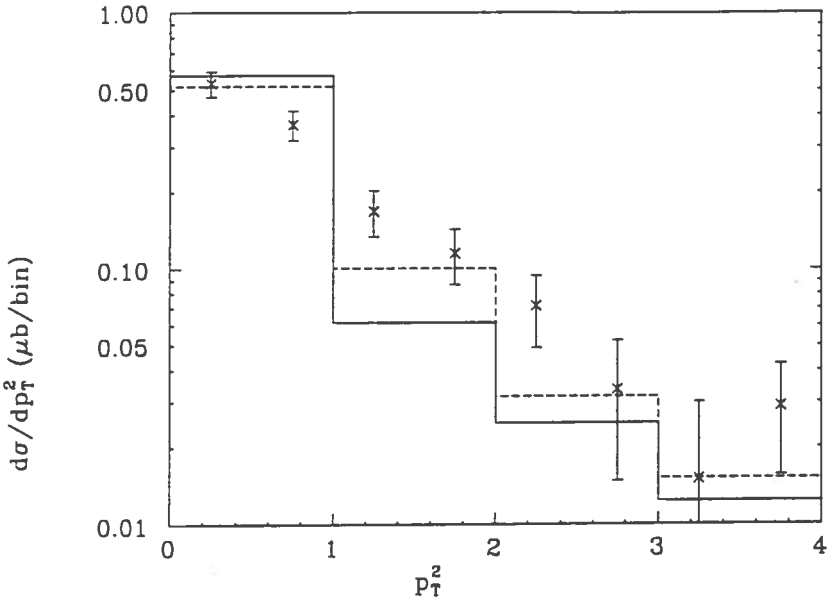

Fig. 1 - $p_t^2(D\overline{D})$. The crosses correspond to the experimental data (E687). The solid and dotted lines are the theoretical previsions: NLO and NLO with gluon $<p_t^2>$=0.5 $(GeV/c)^2$, respectively.

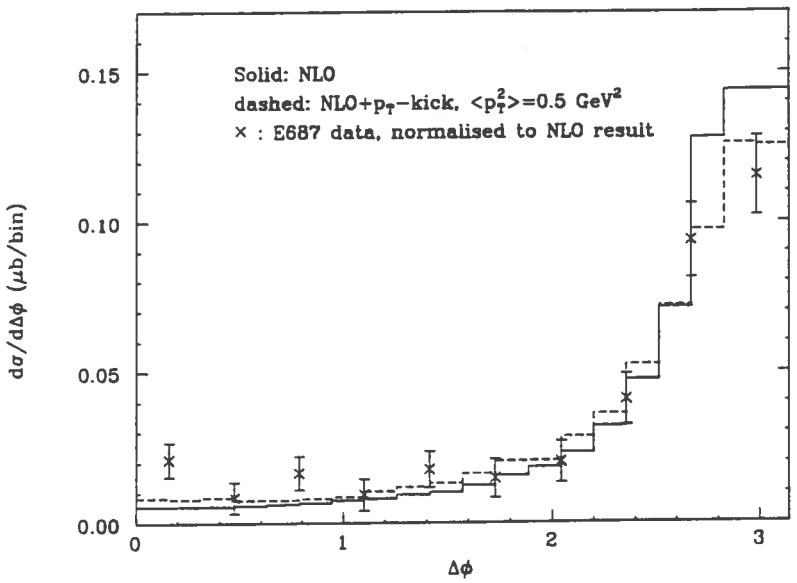

Fig. 2 - Acoplanarity angle. The experimental data are from E687. Legend as in Fig. 1.

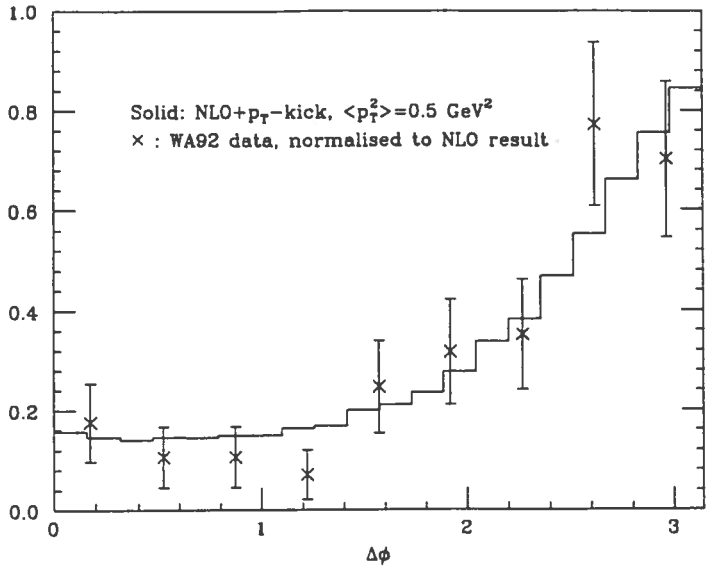

Fig. 3 - Acoplanarity angle. Crosses: WA92 data. Solid line: NLO with a $< p_t^2 >= 0.5 (GeV / c)^2$.

In the selection of the sample $D_s^{\pm} \to \phi\pi^{\pm}[\phi \to K^+K^-; 1.010 < M(K^+K^-) < 1.030\ GeV / c^2]$, the signal to noise ratio was further improved by requiring $|\cos\vartheta| > 0.3$, where ϑ in the angle between one of the kaons and the pion in the ϕ rest frame. This angle follows a $\cos^2$ distribution as a consequence of a decay of a pseudoscalar (D_s) into a vector and a pseudoscalar (ϕ, π).

3.2 Procedure

The use of the "reduced proper time" and the choice of the "binned maximum likelihood" method are two important steps of the procedure followed in order to measure the lifetimes.

The "detachment" cut ℓ/σ_ℓ is largely used as an important tool to disentagle the signal; but it distorts the exponential distribution of the measured proper time, which could be corrected by an heavy use of the Monte Carlo simulations. A better solution is to replace the proper time with the reduced proper time $t' = (\ell - N\sigma_\ell)/\beta\gamma c$, which nearly restores the exponential, thus minimizing the Monte Carlo corrections and then the systematic errors induced by the simulation. A distribution like $f(t')e^{-t'/\tau}$ is used in the fits, where $f(t')$ is a correction function, which takes into account the geometrical acceptance, the analysis cuts, the absorption in the target, the decay of charm secondaries.

Another important tool to minimize the systematic errors is the use of the binned maximum likelihood method which avoids a modelling of the background. Following this method, the t' distribution of the events present in two sidebands (data above and below the particle mass peak) are fitted and the result is used to determine the background underneath the signal.

The predicted number of events n_i in a t' bin is given by:

$$n_i = (N_S - B)\frac{f(t_i')e^{-t_i'/\tau}}{\Sigma f(t_i')e^{-t_i'/\tau}} + B\frac{b_i}{\Sigma b_i}$$

where s_i and b_i are the observed numbers of events in a t' *bin* i of the signal and of the side band histograms, respectively; N_S and B are the total number of events and the number of background events, respectively, in the signal region.

The relation between B and the background events expected from the side bands is assured by the factor ζ_{bg} included in the likelihood function.

The likelihood function is given by:

$$\zeta = \zeta_{signal} \times \zeta_{bg},$$

where

$$\zeta_{signal} = \prod_{i=1}^{\pi} \frac{n_i^{s_i}}{s_i!} \exp(-n_i)$$

$$\zeta_{bg} = \frac{(n_{bg})^{N_{bg}}}{N_{bg}!} \exp(-\mu_{bg})$$

with : $N_{bg} = \Sigma b_i$ and $\mu_{bg} = B/R$; R is the ratio between the widths of the signal and sideband mass regions.

In the fit: τ and B are assumed as free parameters; $S = (N_s - B)$ is constrained to be the total number of signal events.

Using this procedure the background level is jointly determined in the same time by the invariant mass distribution and the t' evolution in the sidebands.

3.3 Study of the systematic effects

Systematic effects have been studied very carefully in this analysis. We discuss here the main error sources:

- influence of the various cuts, especially the detachment cut;
- uncertainties in the correction function $f(t')$;
- uncertainties in the target absorption corrections. Two effects are relevant in this case: the elastic scattering of charm secondaries (and then to what extent it causes mismeasurements of the parent D) and the D absorption in the target (uncertainty on the cross section);
- possible differences between the assumed D momentum distribution in the Monte Carlo and the true distribution;
- uncertainty in the actual proton beam profile at the target: the beam profile determines the relative numbers of events occurring in the microvertex central and outer resolution regions;
- particular choice of sidebands.

Consistency checks have been carried out also for the effects of charm reflection subtraction, absolute vs reduced proper time, used binning, etc...

The detachment cut does not influence significantly the fitted lifetime. $f(t')$ introduces very small corrections; its value is very close to 1.0 in the full t' range. Just as an example $\tau vs\, \ell/\sigma_\ell$ and $f(t')\ vs\ t'$, as obtained in the D_s analysis, are displayed in Figs. 4 and 5. In Table I individual contributions to the systematic errors for the D^0 samples are shown.

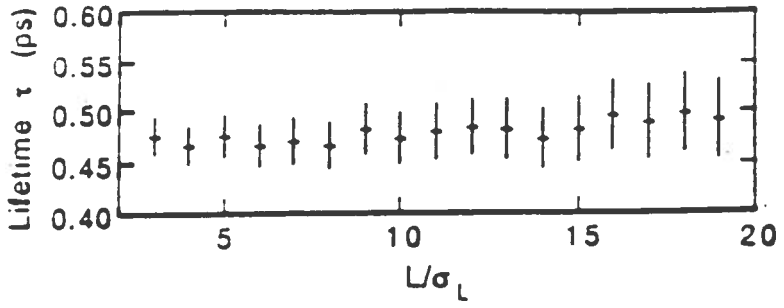

Fig. 4 - $\tau(D_s)$ *vs* ℓ/σ_ℓ. The errors are statistical.

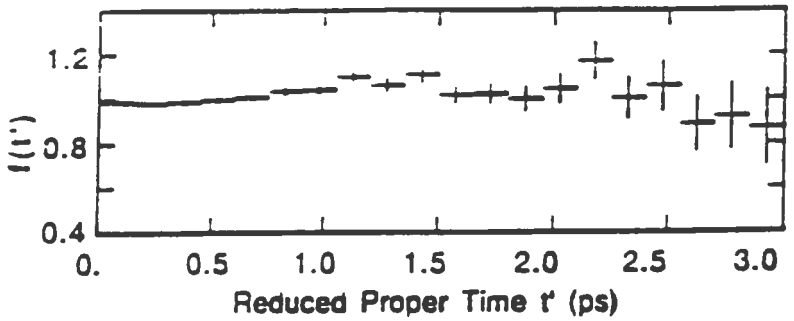

Fig. 5 - The correction function $f(t')$ *vs* t'.

Table I: D^0 lifetime systematics

Source	$K\pi$ Tag	$K\pi$ No Tag	$K3\pi$ Tag	$K3\pi$ No Tag
Beam profile	.0010	.0010	.0010	.0010
Absorption	.0010	.0010	.0010	.0030
Sidebands	.0020	.0060	.0020	.0020
$f(t')$	.0031	.0035	.0030	.0033
Total	.0040	.0070	.0040	.0050

The result of the consistency checks shows that the various lifetime values are always within $\pm\sigma_\tau$ around the quoted result of the analysis. The result of the D_s systematic studies is shown, as an example, in Fig. 6.

3.4 Results

The samples used to measure the lifetime consisted of: 9130 $D^{\pm}$, 16730 $D^0/\overline{D}^0$ (four subsamples), 900 D_s.

The D^0 result is the weighted average of the four statistically independent samples mentioned in §3.. The individual results are shown in Table II.

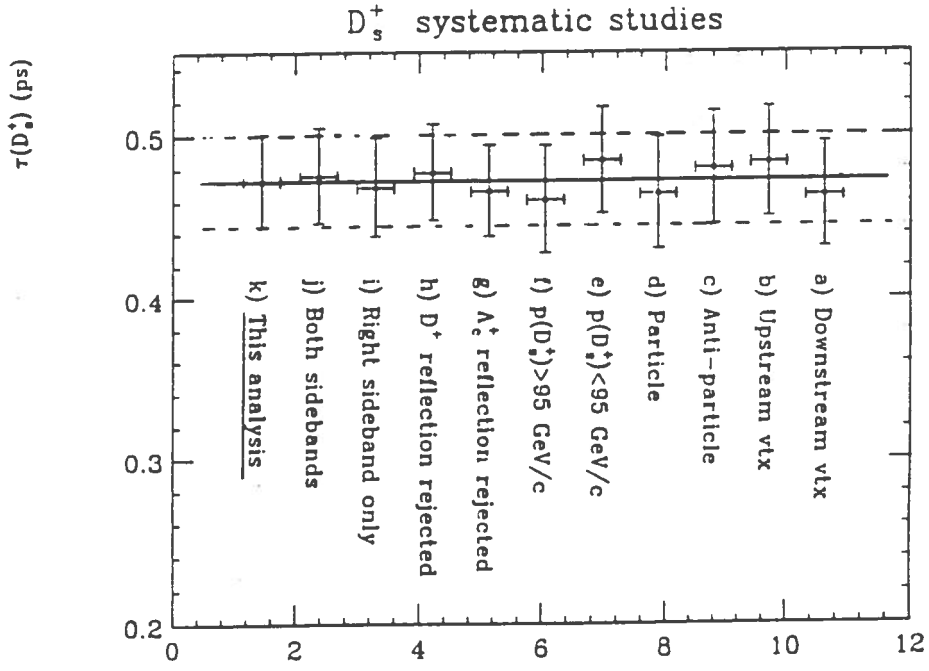

Fig. 6 - Study of systematic effects for the D_s^+ lifetime measurements.

Table II

Sample	Lifetime (x10^{-12}) sec
$K\pi$ Tag	.421±.009±.004
$K\pi$ No Tag	.405±.010±.007
$K3\pi$ Tag	.410±.010±.004
$K3\pi$ No Tag	.413±.007±.005

The final results are quoted in Table III[5,6].

Table III

	E687 λ (psec)	PDG92 λ (psec)	Accuracy (E687)	Accuracy (PDG92)
$D^{\pm}$	$1.048 \pm .015 \pm .011$	$1.066 \pm .023$	1.8%	2.2%
D^{o}	$.413 \pm .004 \pm .003$	$.420 \pm .008$	1.2%	1.9%
$D_s^{\pm}$	$.475 \pm .020 \pm .007$	$.450^{+.030}_{-.026}$	4.5%	6.7%

On the basis of these results we can quote:

$$\frac{\tau(D^{\pm})}{\tau(D^0)} = 2.54 \pm 0.04 \text{ and } \frac{\tau(D_s^{\pm})}{\tau(D^0)} = 1.15 \pm 0.5.$$

4. Hadronic decays

In this section we present some of the results achieved by the E687 collaboration on the hadronic decays. We will discuss: Cabibbo suppressed decays, decays to non strange states, analysis of substructures.

4.1 $D^0 \to K^+K^-$ and $\to \pi^+\pi^-$

Both these channels proceed via similar diagrams: spectator Cabibbo suppressed and exchange. Then, taking into account phase space differences, we expect $\frac{\Gamma(D^0 \to K^+K^-)}{\Gamma(D^0 \to \pi^+\pi^-)} \sim 0.86$. Theoretical models[7], taking into account SU(3) breaking, predict ~1.4.

We selected yields consisting of: 580 ± 39 events for K^+K^-, 179 ± 31 events for $\pi^+\pi^-$. A tight $\check{C}$ identification is required, especially for $\pi^+\pi^-$ mode, to reject the reflection from $D^0 \to K^-\pi^+$ decays. Good confidence levels for the primary and secondary vertices are required; isolation cuts are applied to the primary and secondary vertices. $\ell/\sigma_\ell > 8$ is required for the detachment.

For the systematic errors, three significant contributions are considered: uncertainty in the MC simulation of the $\check{C}$ system, uncertainty due to hadronic interactions of secondaries in the target, variation in yields due to different background parametrizations.

Finally we quote:

$$\frac{\Gamma(D^0 \to K^-K^+)}{\Gamma(D^0 \to \pi^-\pi^+)} = 2.53 \pm 0.46 \pm 0.19$$

This result is compared with the previous ones in Table IV.

Table IV

Experiment	$\frac{B(D^0 \to K^- K^+)}{B(D^0 \to \pi^- \pi^+)}$
Mark II	3.4±1.8
Mark III	3.7±1.4
ARGUS[8]	2.5±0.7
CLEO[9]	2.35±0.37±0.28
E691[10]	1.95±0.34±0.22
WA82[11]	2.23±0.81±0.46

Possible explanations of this anomaly are based upon the significant role that final state interactions could play or on a possible interference between spectator and penguin diagrams, which should be positive for (K^+K^-) and negative for $(\pi^+\pi^-)$.

4.2 D^+, D_s^+ decays into $K_s^0 K^+$ and $K_s^0 \pi^+$.

One C.S. spectator diagram contributes to $D^+ \to \overline{K^0} K^+$, while two Cabibbo allowed diagrams give contribution to the $D^+ \to \overline{K_s^0} \pi^+$, with possible destructive interferences.

BSW quark factorization model[7] predicts $B(D^+ \to \overline{K^0} K^+)/B(D^+ \to \overline{K^0} \pi^+) = 0.33$. Kamal and Verna[12] in the frame of the SU(3) scheme, take into account also final states interactions (FSI), assuming that they simply rotate the amplitudes. Also SU(3) breaking enters in the calculation through FSI. They find 0.26.

The BSW model gives 0.19 for $\frac{B(D_s^+ \to K^0 \pi^+)}{B(D_s^+ \to \overline{K^0} K^+)}$, while Kamal and Verna find 0.068. If in the Kamal and Verna model FSI and SU(3) symmetry breaking are neglected, the results are very similar to the BSW model for both the previous B.R..

We have analyzed both $K_s^0 K^+$ and $K_s^0 \pi^+$ channels. In the selection standard cuts are applied. Systematic studies analyzed the effects of the various cuts, the reflections and the uncertainties of the fitting.

In addition effects of further selections based upon: a cut on the impact parameter vector of the bachelor π or K in the charm decay plane, a cut on the lifetime (<5 D_s^+ and D^+ lifetimes, respectively) and a total isolation cut, have been investigated to control the signal behaviour.

Signal yields are shown in Figs. 7,8 and in Table V. If we interpret the 2σ enhancement of $D_s^\pm \to K_s^0 \pi^\pm$ as a signal, we can quote the BR (Table VI) and compare than with previous data.

All the quoted results are still very preliminar.

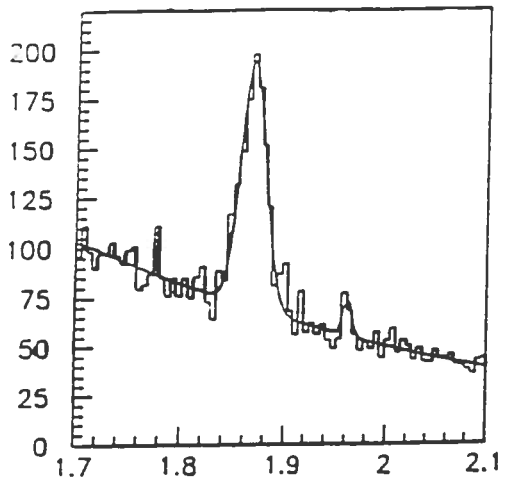

Fig. 7 - $K_s^0\pi^\pm$ invariant mass distribution.

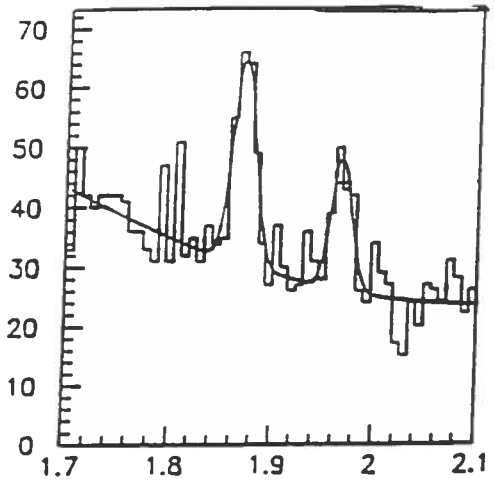

Fig. 8 - $K_s^0K^\pm$ invariant mass distribution.

Table V

Channel	Signal Yield
$D^\pm \to K_s^0\pi^\pm$	702.6±37.7
$D_s^\pm \to K_s^0\pi^\pm$	36.8±14.0
$D^\pm \to K_s^0K^\pm$	129.2±18.3
$D_s^\pm \to K_s^0K^\pm$	75.6±15.2

Table VI

B.R.	Present analysis	Previous measur.
$\frac{D^+ \to \overline{K^0}K^+}{D^+ \to \overline{K^0}\pi^+}$	0.25±0.04	0.27±0.07 (E691)[13] 0.28±0.06 (PDG '92)
$\frac{D_s^+ \to K^0\pi^+}{D_s^+ \to \overline{K^0}K^+}$	0.33±0.14	<0.21(PDG '92)

4.3 Decays to non strange states

The D and D_s can decay into non strange states, as 3π, 4π (in case of D) and 5π, via a Cabibbo suppressed spectator process (as in the case of $D^{\pm}$ and D^0) and an annihilation diagram (as for $D_s^{\pm}$). In the case of D_s, the decay mechanism can be only a Cabibbo allowed annihilation process if the secondary particles do not give origin to resonant substructures, while a Cabibbo suppressed spectator mechanism gives contribution in case of a two body resonant final states.

The E687 collaboration is analyzing these three channels. The analysis of the CS $D^0 \to K^-K^+\pi^-\pi^+$ and of $D^0 \to K^-K^+K^-\pi^+$ is also done in parallel.

4.3.1 The $3\pi^{\pm}$ channel

In the identification of the 3 π channel, the E687 collaboration , in addition to the usual cuts (secondary vertex CL, detachment $\ell/\sigma_\ell > 10$, $\check{C}$ identification, point back cut, etc..), makes use of the requirement that the decay vertex lies outside the target. This last constraint was a very strong tool in improving the signal to noise ratio.

In Fig. 9 the 3π invariant mass distribution, as obtained by E687, is shown. From left to right, the misidentified $K\pi\pi$ reflection, the D and the D_s peaks are clearly evident. A fit done with two Gaussians (we exclude the peak due to the reflection) plus a polynomial gives 179.2 ± 21.1 and 54.2 ± 12.3 for the $D^{\pm}$ and $D_s^{\pm}$ yield, respectively.

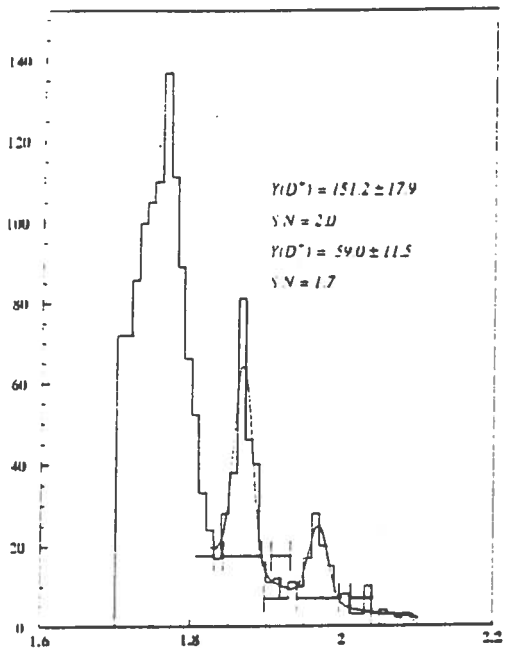

Fig. 9 - $3\pi^{\pm}$ invariant mass distribution.

The reflection of the decays: $D^{0*} \to D^0\pi$ where $D^0 \to K^-\pi^+$ (K misidentified as π) and $D^{*+} \to D^0\pi^+$, where $D^0 \to \pi^+\pi^-$, were carefully studied and the fake events have been kinematically

removed. The effects of this rejection have been studied by means of a MC simulation, using the D^* BR quoted in PDG '92. Anyway they do not introduce dishomogeneities on the Dalitz plot.

A Dalitz plot analysis is now being analyzed for the $D_s \to 3\pi$ signal. Events falling within 2σ of the D_s^+ mass peak are considered for the D_s Dalitz plot, while the sidebands are defined as indicated in Fig. 9. To extract the fraction of the resonant components, a maximum likelihood fit is applied to the folded Dalitz plot of $(M^2_{\pi^+\pi^-})_{high}$ vs $(M^2_{\pi^+\pi^-})_{low}$.

The total amplitude used in the probability function is a coherent sum of three resonances [ρ (770), f_0 (975), f_2 (1270)] plus a flat non-resonant contribution:

$$A_T = A_{NR} + C_\rho A_\rho e^{i\phi_\rho} + C_{f_2} A_{f_2} e^{i\phi_{f_2}} + C_{f_0} A_{f_0} e^{i\phi_{f_0}}$$

In the context of the helicity formalism, each resonance amplitude has the form:

$$A_r(m_{12}^2, m_{13}^2) = \sqrt{\frac{M_D}{p_r}} \sqrt{\frac{m_{12}}{p_\pi}} \times f(\cos\vartheta_3) \times BW$$

where: p_r= momentum of the resonance r in the r r.f.
p_π= momentum of one of the two pions in the r r.f.
m_{12}= lowest ($\pi\,\pi$) mass.

BR is a P wave Breit Wigner function:

$$BW_r = \frac{m_r \sqrt{\Gamma_r}}{(m_r^2 - m_{12}^2) - i m_r \Gamma_r} \qquad \Gamma_r = \Gamma_0 \left(\frac{p_\pi}{p_r}\right)^{(2J+1)},$$

p_π= momentum of a pion in the r r.f..

In case of $J = 0$, we simply assume $\Gamma_r = \Gamma_0$.

In the particular case of f_0 a coupled channel BW has been assumed[13]:

$$BW_{f_0} = \frac{m_{f_0} \sqrt{\Gamma_\pi}}{(m_{f_0}^2 - m_{12}^2) - i m_{f_0} (\Gamma_\pi + \Gamma_K)}$$

where:

$$\Gamma_\pi = g_\pi \left(\sqrt{\frac{m_{12}^2}{4} - m_\pi^2} \right)$$

$$\Gamma_K = g_K \left(\sqrt{\frac{m_{12}^2}{4} - m_K^2} + \sqrt{\frac{m_{12}^2}{4} - m_{K^0}^2} \right)$$

Special care has been devoted to the treatment of the background. Two different approaches have been used and tested:

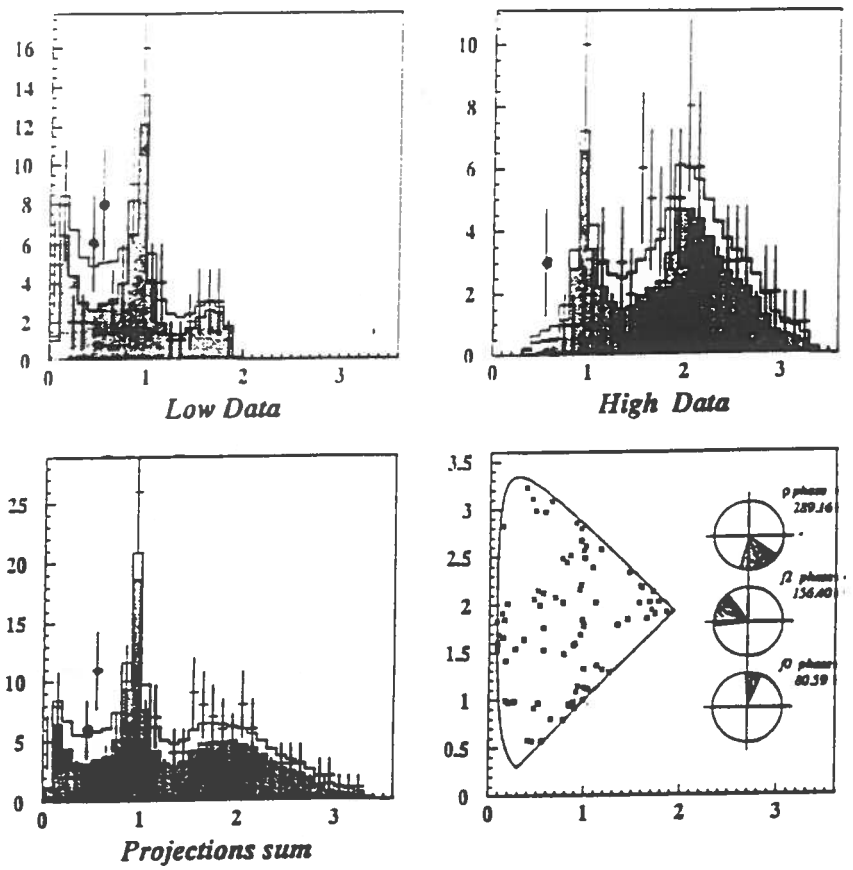

Fig. 10 - Analysis of $D_s^{\pm} \to \pi^{\mp}\pi^{\pm}\pi^{\pm}$. Real data: error bars; fit results: full line; model amplitude computed with the resulting fit parameter: shaded.

- the background contribution to the signal region has been properly subtracted using events from the sidebands (likelihood subtraction- LS);
- the background in the signal region has been parametrized using events from the sidebands (sideband modeling - SM).

We finally preferred the SM approach because stronger from the statistical point of view.

In Fig. 10 the Dalitz plot with the low and high projections are presented. The fit is done using the SM strategy.

Preliminary results show that the f^0 component is dominant.

4.3.2 4π, $2K2\pi$, $KKK\pi$ channels

E687 is analyzing the following channels:

i - $D^0 \to \pi^+\pi^-\pi^+\pi^-$

ii - $D^0 \to K^-K^+\pi^-\pi^+$

iii- $D^0 \to K^-K^+K^-\pi^+$

The first two channels can go via a CS spectator mechanism; the last one is a Cabibbo allowed, but it is strongly depressed by the phase space. Usual cuts have been used in this analysis: $\check{C}$ identification, confidence level for the primary and secondary vertices, detachment and point back cuts, etc.. An important reflection peak is present in i) and ii); it is due to a misinterpretation of the channel ($K\,3\pi$) where the kaon is interpreted as a π (~1.75 GeV bump in the 4 π mass distribution) or a π is misidentified as a kaon (~1.98 GeV bump in the $2K\ 2\pi$ mass distribution).

The signals are shown in Fig. 11. They are fitted by Gaussians plus a polynomial. The yields consist of: 814±52 events for (4π) channel, 259±29 events for ($2K\ 2\pi$), 20±5 events for ($3K\ \pi$).

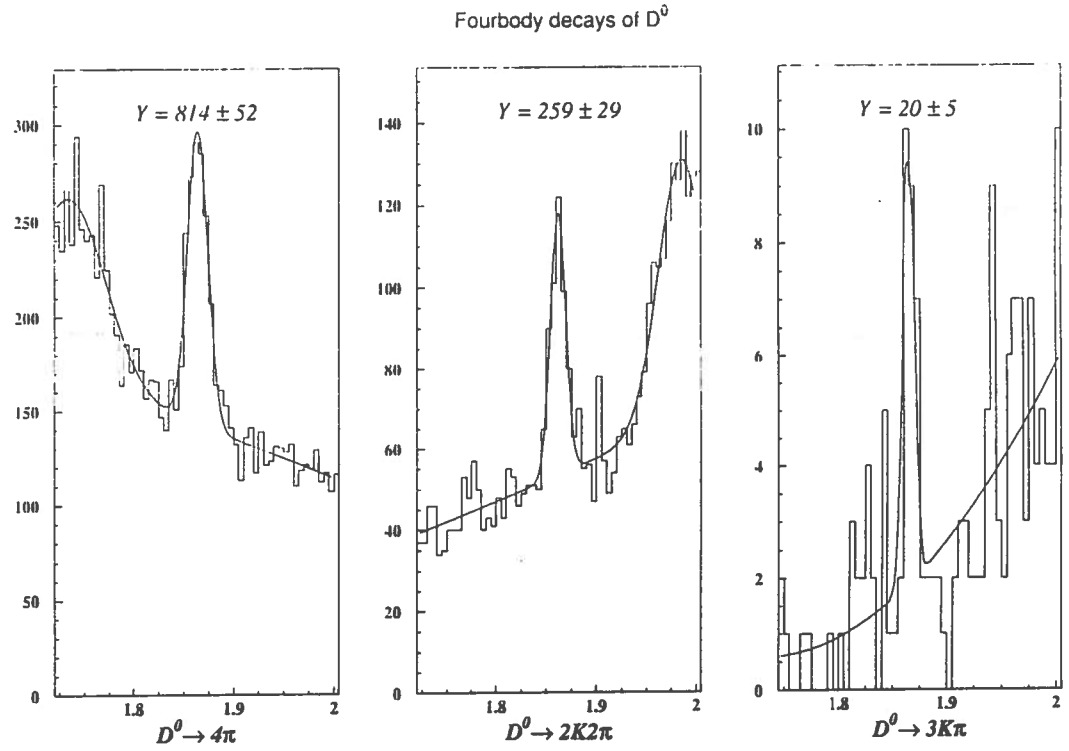

Fig. 11 - Four body invariant mass distributions (GeV).

The preliminary results of this analysis are presented in Table VII, where they are compared with previous results.

From our results we obtain:

$$\frac{\Gamma(D^0 \to 2K\,2\pi)}{\Gamma(D^0 \to 4\pi)} = 0.36 \pm 0.05 \pm 0.02$$

The first error is statistical; the second one is systematic. The main contribution to the systematic error is due to changements in the fit as a consequence of different parametrizations of the peaks and background.

The dependence of the BR on the various cut values used in the analysis (vertex confidence levels, isolations, detachment, pointback, etc..) has been studied . The result is a very stable behaviour when the cuts are changed. We do not expect systematic effects from the cuts.

Table VII

B.R.	E687	Previous results
$\frac{\Gamma(D^0 \to 4\pi)}{\Gamma(D^0 \to K3\pi)}$	$0.097 \pm 0.006 \pm 0.002$	$0.096 \pm 0.018 \pm 0.007$ (E691)[14] 0.102 ± 0.013 (CLEO)[15]
$\frac{\Gamma(D^0 \to 2K2\pi)}{\Gamma(D^0 \to K3\pi)}$	$0.035 \pm 0.004 \pm 0.002$	$0.028^{+0.008}_{-0.007}$ (E691)[14] 0.0314 ± 0.010 (CLEO)[15] $0.041 \pm 0.007 \pm 0.005$ (ARGUS)[16]
$\frac{\Gamma(D^0 \to 3K\pi)}{\Gamma(D^0 \to K3\pi)}$	$0.0028 \pm 0.0007 \pm 0.002$	

We have to note that we observe $D^0 \to 4\pi$ (no strange particles) with a BR more than twice that of $D^0 \to 2K2\pi$ (two strange particles) whereas $D^0 \to 2\pi$ (no strange particles) has a BR less than half that $D^0 \to 2K$ (two strange particles) (see §4.1). This asymmetry shows, once again, that simple spectator decays do not dominate; in that case infact a quark-level symmetry should be expected.

4.3.3 5π channel

E687 found the first actual evidence of D, D_s decay into 5π. As in the case of the 3π analysis, the requirement that the secondary vertex will be downstream of the target gave an important help in disentangling the signal. The fitted yields (very preliminary) consist of 40 ± 7 and 24 ± 5 events for $D^{\pm}$ and $D_s^{\pm}$, respectively (see Fig. 12).

The reflection from the $K\ 3\pi$ signal, where the kaon is misidentified as a π, is present in the low mass region of the plot (<1.8 GeV).

In a previous analysis E691 gave only upper limits

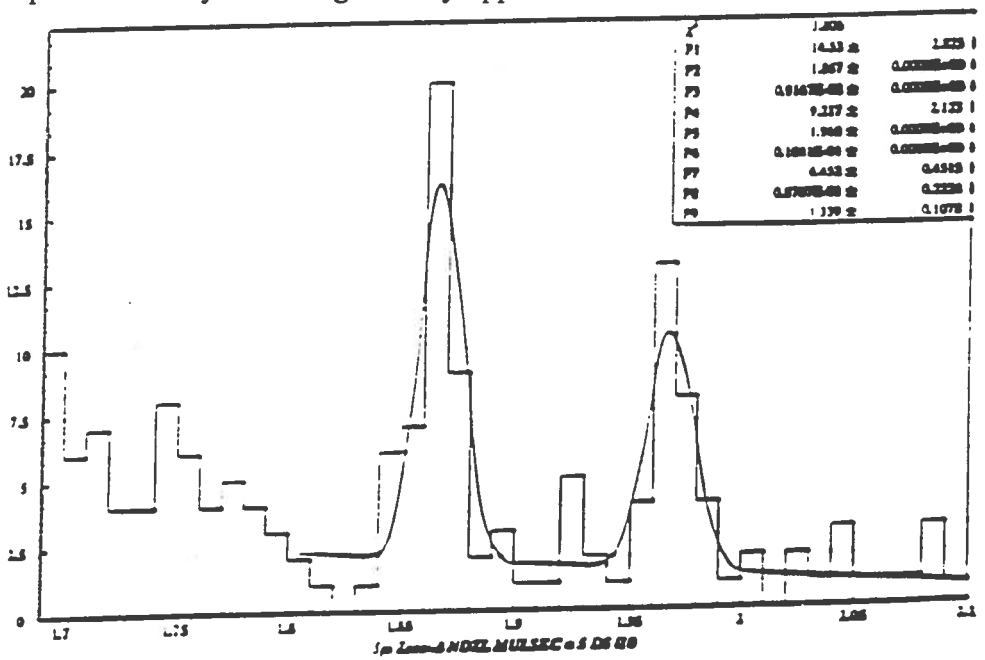

Fig. 12 - 5π mass plot (GeV).

4.4 Search of substructures

The E687 collaboration has done a very extended analysis of the Dalitz plots for the channels $K\,\pi\,\pi$ and $K\,K\,\pi$.

The $K\,\pi\,\pi$ analysis is based upon a formalism, which uses essentially the Zemach method. The results were anyway checked also by means of the helicity formalism. In this analysis the formalism was extended to allow for the possibility of contributions from all known $(K\,\pi)$ and $(\pi\,\pi)$ resonances.

For the $K\,K\,\pi$ analysis the helicity formalism is used, similarly as in the analysis of the 3π channel (see section 4.3.1). This is the first time that a full coherent Dalitz plot amplitude analysis is done on the $K\,K\,\pi$ final state.

The fits are performed both with 3 amplitudes (non-resonant, $\phi,\overline{K^{*0}}$) and with 4 amplitudes (f_0 [975] is added).

4.4.1 The $K\,\pi\,\pi$ analysis[17]

The channels analyzed by our collaboration are: $D^0\to K^0_s\pi^+\pi^-, D^+\to K^-\pi^+\pi^+, D^0\to K^-\pi^+\pi^0$.

The $D^0\to K^0_s\pi^+\pi^-$ was $D^{*+}(\to D^0\pi^+)$ constrained . [$D^{*+}-D^0$ mass difference within 2 MeV of the accepted value]. In addition to the usual cuts, a cut on the momentum (>45 GeV/c) of the $(K^0_s\pi^+\pi^-)$ combination helps in improving the signal/noise ratio, while the requirement that the K^0_s vertex would be downstream of the D^0 vertex by at least 3 standard deviations removes possible contaminations from $D^0\to 4\pi^{\pm}$.

For the decay $D^+\to K^-\pi^+\pi^+$ decay mode, the possible background from the decay $D^{*+}\to D^0\pi^+, D^0\to K^-\pi^+\pi^0$ is avoided by excluding the contaminated regions [low $m^2(\pi\pi)$ and $m^2(K\pi)$] from the analysis.

The $D^0\to K^-\pi^+\pi^0$ was D^* constrained as in the case of the $D^0\to K^0_s\pi^+\pi^+$. The π^0's are reconstructed using the e.m. calorimeter; the cut $0.09<M(\pi^0)<0.16\ GeV$ has been adopted. Also in this case a requirement on the $K^-\pi^+\pi^0$ momentum (>70 GeV/c) was applied to improve the signal/noise.

For the Dalitz plot analysis, events having invariant mass in the region $\pm 2\,\sigma$ from the signal peak were selected for the Dalitz plot fit. Events from the sidebands ($4\,\sigma$ width separated by $2\,\sigma$ below and above the signal region) were used to evaluate the background below the signal. For the $(K^-\pi^+\pi^0)$ channel, because the invariant mass resolution is a strong function of the D^0 energy carried out by the π^0, the selection is based upon the normalized invariant mass, $\frac{M(K^-\pi^+\pi^0)-M_{D^0}}{\sigma}$, which is required to be less than 2.

In Fig. 13a,b,c the invariant mass plots for the three channels are shown. The background is always very low. The fitted yields consist of: 597 ± 26 events for $(K^0_s\pi^+\pi^-)$, 8800 ± 97 events for $(K^-\pi^+\pi^+)$ and 530 ± 30 events for $(K^-\pi^+\pi^0)$.

In Fig. 14, the Dalitz plots, their projections and the fit results are illustrated.

The fitted decay fractions, the relative phases and the BR are presented in Table VIII. The decay fraction of a mode is computed by integrating the signal intensity for that mode, divided by the integrated intensity for all modes. These fractions do not sum to one due to the presence of interference between the modes. The BR are calculated simply by multiplying the decay fractions by the BR for the three-body final state and dividing for the $(K\,\pi)$ or $(\pi\,\pi)$ resonance where appropriate.

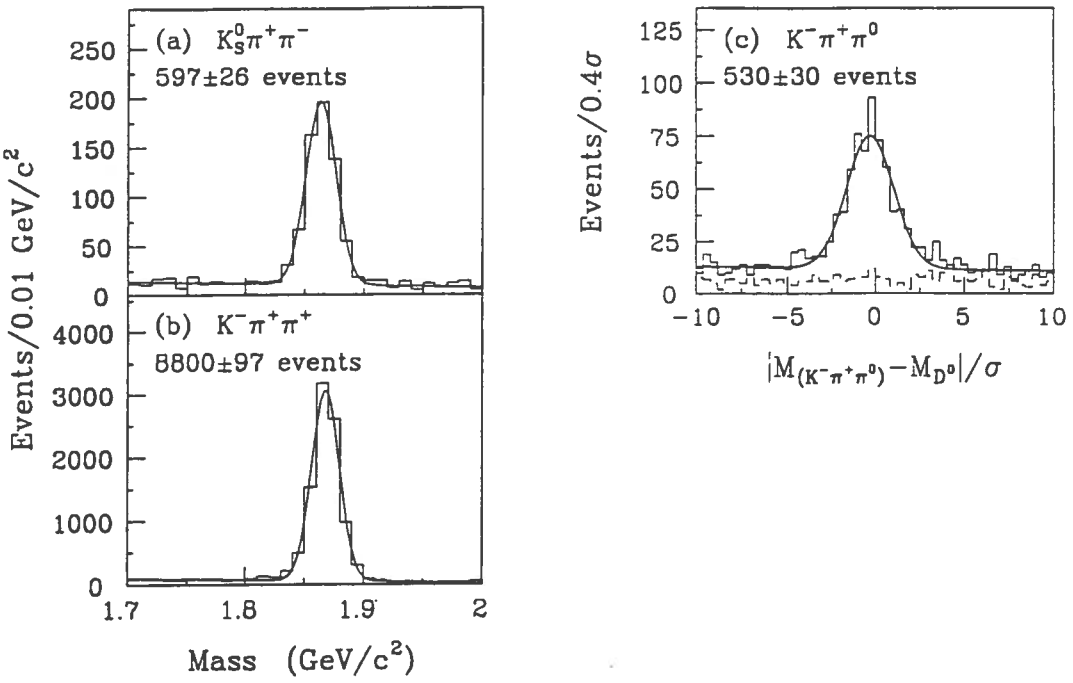

Fig. 13 - Invariant mass distributions for the three $D \to K\pi\pi$ decay modes. In (c) the normalized mass difference is plotted (see the text). All fits are done with a Gaussian distribution and a linear background function.

The quotes errors are statistical (first set) and systematic (second and third sets). The second error set takes into account the uncertainties in the background subtraction and evaluation, fitting procedures, etc.. The third set of errors arises from the uncertainties in the ($K\ \pi$) and ($\pi\ \pi$) resonance shapes and in the assumed mixture of contributing ($K\ \pi$) and ($\pi\ \pi$) resonances.

The most important aspect of these results is the big difference of the non resonant contributions between D^0 and $D^\pm$ channels; this is surprising because all three channels decay via similar diagrams. The $D^0 \to K^-\pi^+\pi^0$ final state is well described by a sum of intermediate two-body resonances, without any appreciable contribution of non-resonant ; the $D^0 \to K^0_s\pi^+\pi^-$ is approximately represented by intermediate two-body resonant decays with a small, but not negligible, non-resonant contribution; the $D^+ \to K^-\pi^+\pi^+$ decay mode, on the other hand, is characterized by a very large non-resonant contribution, which strongly dominates the channel.

No clear explanation is presently available to understand these very different behaviours of $D^\pm$ and D^0 channels.

Our results can be compared with the analysis previously done by Argus[18], which studies only $D^0 \to K^0\pi^+\pi^-$, and by E691[19], which analyses all three modes. The agreement with Argus is quite good both for the B.R. and the relative phases. The comparison with E691 data show that there is a fairly good agreement for the BR, while most of the relative phases shows a significant disagreement.

4.4.2 $K\ K\ \pi$ analysis

The E687 collaboration have done for the first time a full coherent Dalitz plot amplitude analysis on the $K\ K\ \pi$ final state.

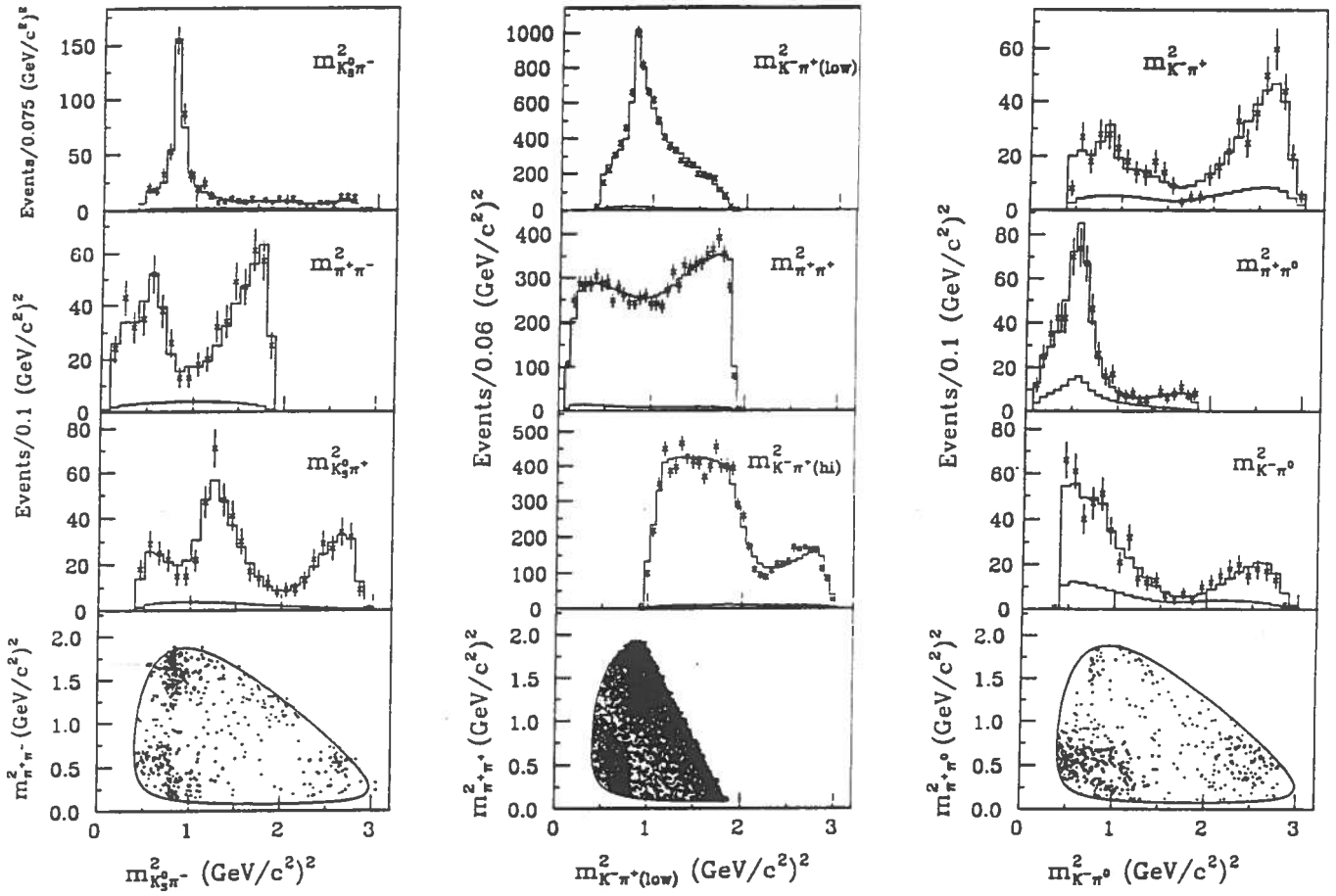

Fig. 14 - Dalitz plots and mass-squared projections for the decays $D^+ \to K^0_s\pi^+\pi^-$, $D^+ \to K^-\pi^+\pi^+$ and $D^0 \to K^-\pi^+\pi^0$ (from left to right). The data are represented by points. In each mass-squared projection the upper histogram describes the predicted signal plus background contribution as determined by the fit, and the lower histogram represents the background contribution.

The sample was selected by means of the usual set of cuts, included the pointback cut. In addition the $K\ K\ \pi$ combinations are rejected if, when reconstructed as $K\ \pi\ \pi$, they fall within 2σ of the D^+ mass. This last requirement removes the $(K\ \pi\ \pi)$ reflection. This method allows to use a mass-dependent efficiency function and then to properly weight the reflection cuts in the Probability Density Function. The effects of the antireflection cuts are well compensated via Monte Carlo simulations.

Possible reflections from $D^{*+} \to D^0\pi^+$, $D^0 \to K^-K^+$ and from $\Lambda_c \to pK^-\pi^+$ are also investigated and are found to be very low. Their influence on the result is found to be negligible.

Table VIII

Dalitz plot fit results for the $D^0 \to K^0_s \pi^+ \pi^-$ final state

Decay mode	Decay fraction	Phase (degrees)	Branching ratio (%)
$K^{*-}\pi^+$	0.625±0.036±0.020±0.016	0.0 (fixed)	5.06±0.29±0.50±0.13
$K^*_0(1430)^-\pi^+$	0.109±0.027±0.028±0.009	-166±11±3±7	0.95±0.23±0.26±0.08
$\overline{K^0}\rho^0$	0.350±0.028±0.045±0.006	-136±6±2±2	1.89±0.15±0.30±0.03
$\overline{K^0}f_0(975)$	0.068±0.016±0.017±0.004	38±11±3±4	0.47±0.11±0.13±0.03
$\overline{K^0}f_2(1270)$	0.037±0.014±0.017±0.002	-174±11±20±42	0.24±0.09±0.11±0.01
$\overline{K^0}f_0(1400)$	0.077±0.022±0.029±0.010	-45±12±21±12	0.44±0.13±0.17±0.06
$\chi^2/(dof)$	2.29 (23 dof)		
Dalitz plot fit results for the $D^+ \to K^-\pi^+\pi^+$ final state			
$\overline{K^{*0}}\pi^+$	0.137±0.006±0.008±0.005	48±2±1±1	1.64±0.07±0.18±0.06
$\overline{K^*_0(1430)^0}\pi^+$	0.284±0.022±0.032±0.049	63±2±3±4	3.66±0.28±0.56±0.63
$\overline{K^*(1680)^0}\pi^+$	0.047±0.006±0.002±0.007	73±4±16±7	1.46±0.19±0.18±0.22
Nonresonant	0.998±0.037±0.046±0.056	0.0 (fixed)	7.98±0.30±0.83±0.45
$\chi^2/(dof)$	3.01 (29 dof)		
Dalitz plot fit results for the $D^0 \to K^-\pi^+\pi^0$ final state			
$K^-\rho^+$	0.765±0.041±0.022±0.049	0.0 (fixed)	8.64±0.46±0.88±0.55
$K^{*-}\pi^+$	0.148±0.028±0.049±0.003	162±10±7±4	5.02±0.95±1.73±0.10
$\overline{K^{*0}}\pi^0$	0.165±0.031±0.011±0.011	-2±12±23±2	2.80±0.53±0.33±0.19
Nonresonant	0.101±0.033±0.030±0.027	-122±10±21±3	1.14±0.37±0.36±0.31
$\chi^2/(dof)$	1.59 (24 dof)		

The mass plot of the selected sample is shown in Fig. 15. The corresponding yields consist of 567.2±28.8 events for $D^\pm$ and 409.1±25.7, for $D^\pm_s$.

The background has been treated by modeling it via a fit on the sideband Dalitz plots using the possible B.W. resonances and polynomial functions. This method was preferred to the background subtraction in the likelihood, because it seems to produce more stable fits.

3-amplitude fits (non-resonant, ϕ, K^{*0}) are performed for both the D and D_s regions. In Fig. 15, the Dalitz plots are presented; in Figs. 16a,b and 17a,b the $m^2_{K^-K^+}$ and $m^2_{K^-\pi^+}$ projections are shown , with the fit results superimposed.

The best fit values of the coefficients, phases and fractions are summarized in Table IX.

The fits results are very stable if we move the cuts, as the detachments, the $\check{C}$ identification. etc..

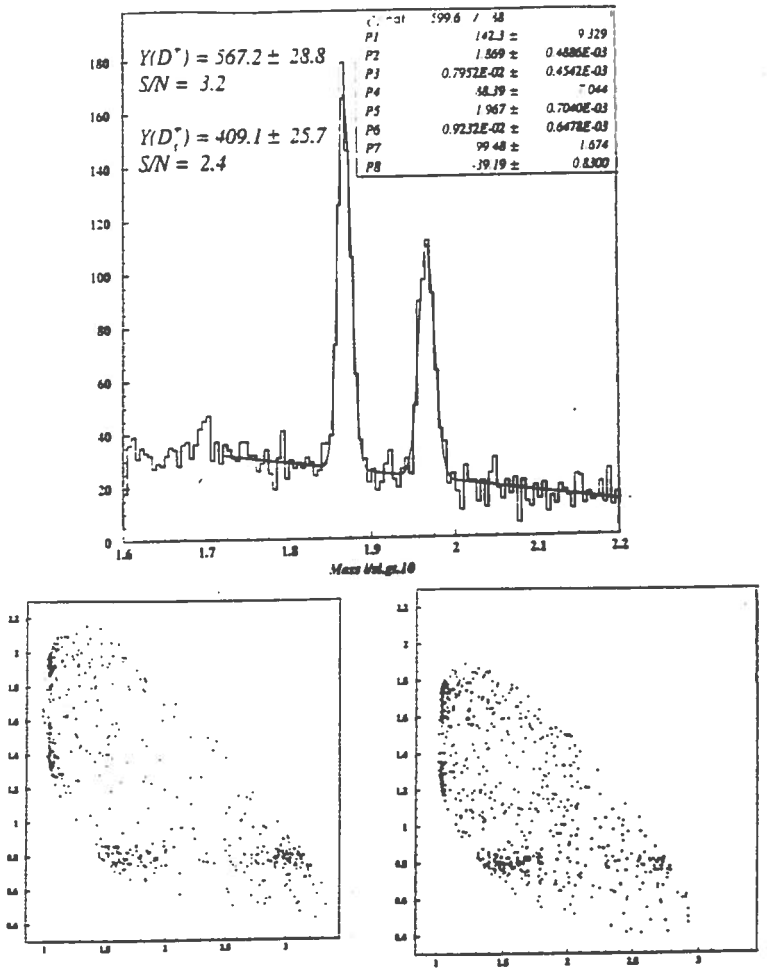

Fig. 15 - Mass distribution for the $K^{\mp}K^{\pm}\pi^{\pm}$ channel and the Dalitz plots for D_s^+ (left) and D^+ (right).

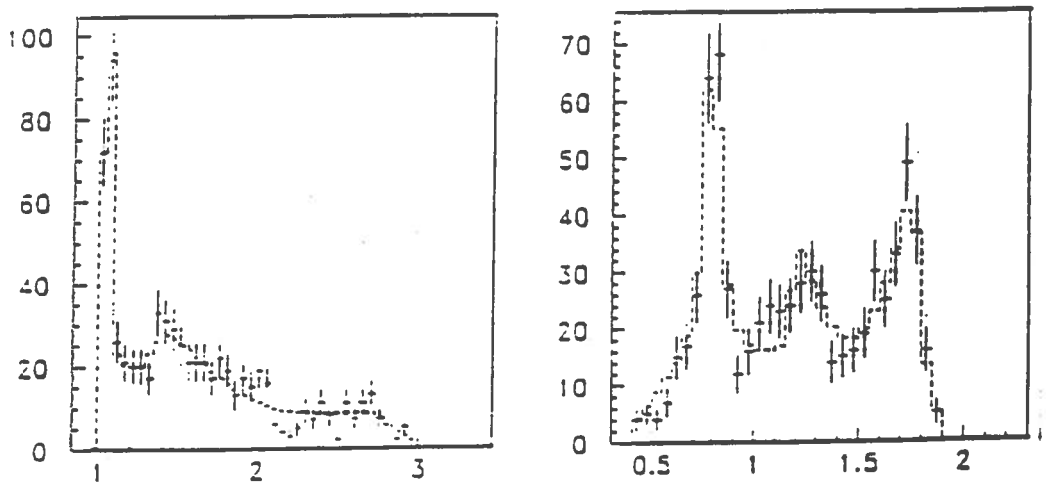

Fig. 16 - D^+ Dalitz plot $m^2_{K^-K^+}$ and $m^2_{K^-\pi^+}$ projections. The histogram corresponds to the fit and the crosses to the data.

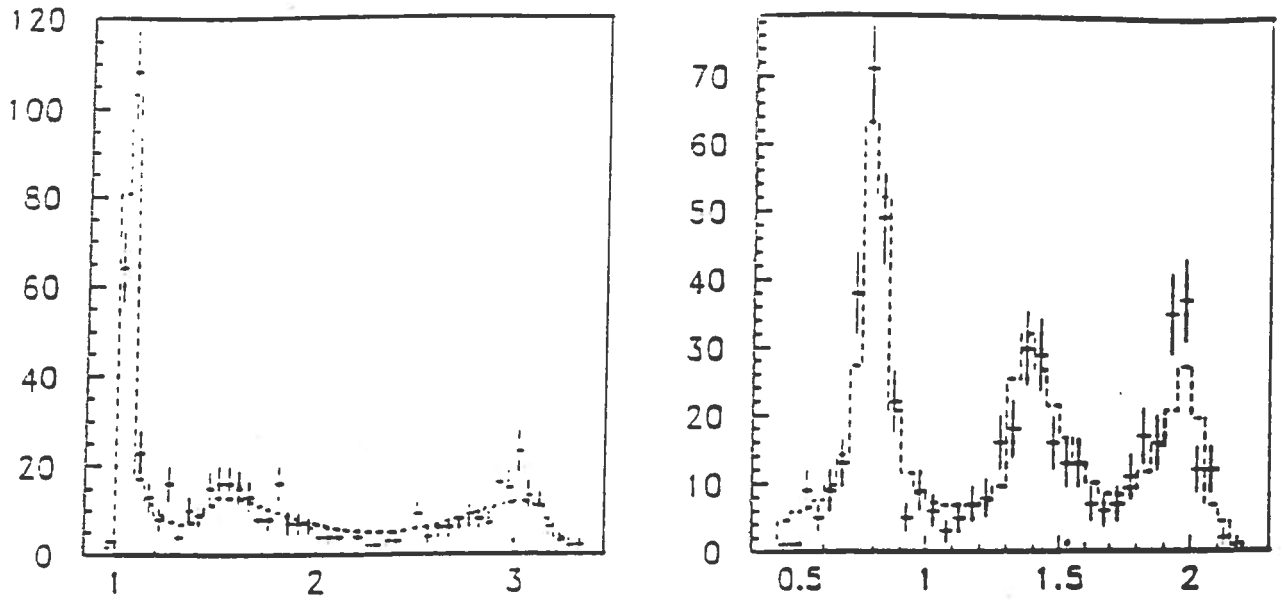

Fig. 17 - D_s^+ Dalitz plot $m^2_{K^-K^+}$ and $m^2_{K^-\pi^+}$ projections. The crosses are the experimental data and the histogram corresponds to the fit.

Table IX
3-amplitude fit results

Fit coefficients and phases	$D_s^{\pm}$	$D^{\pm}$
Nonresonant	0.289±0.058	1.160±0.096
ϕ	0.848±0.048	1.022±0.076
K^{*0}	1.	1.
Non-resonant phase	0.144±0.251	-1.455±0.109
ϕ phase	2.022±0.131	2.979±0.127
K^{*0} phase	0	0
fit fractions %		
non-resonant	5.34±2.00	43.01±3.10
ϕ	45.71±3.25	33.35±2.60
K^{*0}	63.59±3.24	31.95±3.48

We have tried to fit the data also using a 4-amplitude fit, namely by adding to the previous ones the f_0 (975). The shape and the phase of the f_0 are very similar to those of the non-resonant amplitudes. The maximum variation across the Dalitz plot of the f_0 term is small and its phase is nearly constant since, in $K\,K$ state, we do not cross the pole. As a consequence it is difficult to disentangle the two components.

Infact if we perform a 3-amplitude with f_0, the fitted fraction of the f_0 component is very similar to the non-resonant fraction displayed in Table IX.

The results of the 4-amplitude fit are very similar to the 3-amplitude best fit values only for the ϕ and K^{*0} components. On the other hand in the D_s sample the non-resonant and f_0 fractions are pushed up to $77 \pm 36\%$ and $61.46 \pm 19.57\%$, respectively. In the D sample the non-resonant and f_0 fractions are depressed to $6.05 \pm 4.62\%$ and $24.30 \pm 12.48\%$, respectively. The corresponding errors are large, showing once again the difficulty of the likelihood.

The 3-amplitude fits can be compared with an incoherent analysis done by E691 on the same channel[20]. The E691 results concerning the D state show an agreement for the non-resonant component, while the ϕ and K^* fractions are higher than the non-resonant components in E691 analysis and lower in our analysis.

For the D_s^+ results the non-resonant contribution is definitively higher in the E691 than in our analysis.

5. Semileptonic decays

The E687 collaboration analyzed four semileptonic decay channels: $D^0 \to K^- \mu \nu$; $D^+ \to \overline{K^{*0}} \mu \nu$; $D^0 \to K^{*-} \mu \nu$ and $D_s^+ \to \phi \mu \nu$. The analysis of the same channels with an electron instead of a muon in the final state is now in progress.

In the analysis of the semileptonic decays, due to the missed ν, the pointback constraint and the selection on the invariant mass of the final state $(D^{\pm}, D^0, D_s)$ are lost. As a consequence the identification of the signals is more complex. I summarize here the main steps of the analysis:

- $(K^- \mu \nu)$; $D^{*+}(\to D^0 \pi^+)$ tag events are considered; the usual cuts (vertex confidence level, detachment, isolation) are applied to the vertices (the primary vertex is required to have one identified π, at least); imposing $M(K\mu\nu) \equiv M(D^0)$ and assuming the direction between the primary and the secondary vertices as the D flight line, it is possible to calculate p_ν; $|p_\pi \| p_D| \geq \vec{p}_\pi \cdot \vec{p}_D$ is required to decrease the possible soft pion combinatorial; the fit to obtain the yield is done on the $(M_{D^*} - M_D)$ plot; the wrong sign events are subtracted; the fit to the pole mass, in a one pole approximation of the form factor, is done on the q^2 distribution (old analysis).
  A new approach has been adopted recently. In this case a fit to the yield and to the pole mass is done simultaneously by means of a binned Maximum Likelihood function:
  $$L = \Pi \frac{n_i^{s_i} e^{-n_i}}{s_i!}$$
  where: s_i=nb of events in the i bin; n_i is a function of: the number of the misidentified events in the bin i from $K^{*0} \mu^+ \nu$ and $K^{*-} \mu^+ \nu$, the background from misidentified wrong sign events in the bin i, the efficiencies. The fitted distribution is $d\Gamma / dq^2$ (new analysis).

- $(K^* \mu \nu)$: K, π, μ vertices with K, μ, π identified, are selected ; usual vertexing cuts are applied; the yield is obtained by fitting the K^* (982) peak; the wrong sign combinations are subtracted;

- $(\phi \mu \nu)$: $K K \mu$ vertices with K, μ identified are selected; the $M(KK\mu)$ is required to be <1.9 GeV [to reject $(KK\mu)$ background, where a pion is misidentified as a μ]; $p_T^2(\phi)$ has to be >0.05 $(\text{GeV/c})^2$ (to avoid ϕ's diffractively produced); a primary vertex is looked for and all the usual vertexing cuts are applied; the $p(D_s)$ is calculated with a two-fold kinematic ambiguity, assuming

that it points along the line defined by the primary and secondary vertex; the yield is obtained by fitting the $K\,K$ mass distribution.

The contribution of fake events due to misidentification or/and loss of particles is evaluated:
- using Monte Carlo simulations and the BR's given in the literature;
- fitting the mass distributions by means of fit functions based upon Monte Carlo distributions for the signal and the background misinterpreted channels;
- including in the maximum likelihood function a term, which takes into account these sources of background.

The systematic errors are mainly due to uncertainties in the evaluation of the background charm decay modes and, more in general, in the simulation based corrections.

Reality checks of the signals have been carried out, obtaining in general a good agreement with the simulation previsions.

5.1 $D^0 \to K^- \mu \nu$

In Fig. 18 the q^2 and $[M(D^{*-}) - M(D^0)]$ distributions are shown with the results of the Maximum Likelihood fit of the new analysis. The total yield is 472 ± 25 events. A detailed analysis of the systematic effects has been carried out and a good stability of the results, when the cuts are moved, has been found.

The BR's, as measured in the old and new analysis, are shown in Table X, where they are compared with the more recent results. There is a general agreement among the various results.

The results of the pole mass are presented in Table XI.

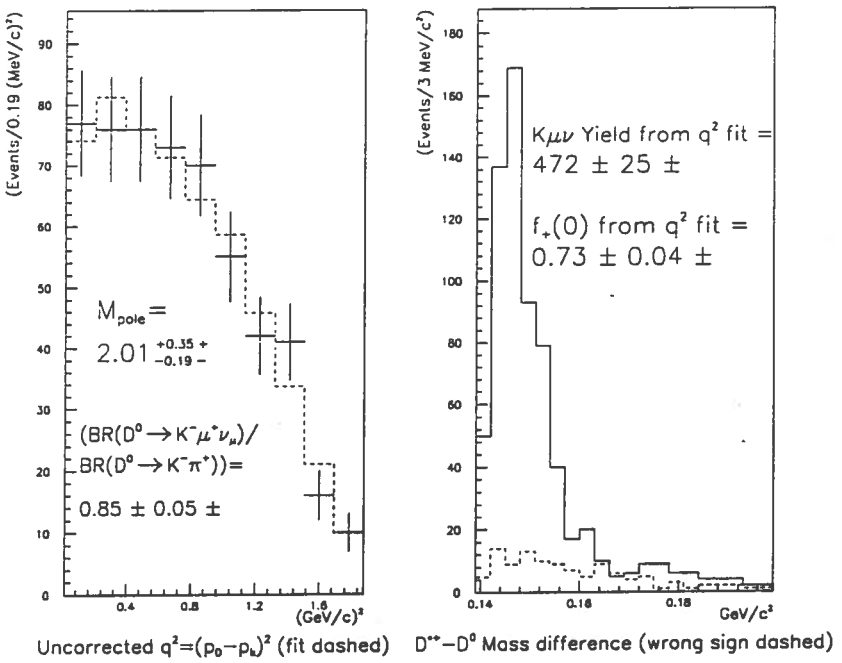

Fig. 18 - The q^2 and $[M(D^{*+}) - M(D^0)]$ distributions, as obtained by E687 ('90-'91) (see text).

Table X

EXPERIMENTS	$\frac{D \to K\ell\nu}{D \to K\pi}$
E687(87-88) (μ)[25]	$0.82 \pm 0.13 \pm 0.13$
E687(90-91) (μ)-old analysis	$0.82 \pm 0.08 \pm 0.09$
E687(90-91) (μ)-new analysis	0.84 ± 0.05
CLEO (μ)[22]	$0.79 \pm 0.08 \pm 0.09$
CLEO(e)[29]	$0.978 \pm 0.027 \pm 0.044$
E691 (e)[23]	$0.91 \pm 0.07 \pm 0.11$

Table XI

Exp.	M_p	$f_+(0)$
E687 (μ)-old analysis	$2.1^{+0.7+0.7}_{-0.3-0.3}$	0.77 ± 0.08
E687(μ)-new analysis	$2.01^{+0.35}_{-0.19}$	0.73 ± 0.04
E691 (e)	$2.1^{+0.4}_{-0.2} \pm 0.2$	0.79 ± 0.05
CLEO[29]	$2.0 \pm 0.12 \pm 0.18$	$0.77 \pm 0.01 \pm 0.04$

The various results agree each to other very well. The best fit value of the pole mass agrees, as expected, with $M(D_s^*)$. The agreement of these results with the theoretical previsions is fairly good, with few exceptions.

5.2 $D^+ \to K^{*0}\mu\nu$

The total yield selected by E687 consists of 875 ± 44 events. The BR with respect to the normalization channel ($K^-\pi^+\pi^+$) and the ratio $\frac{\Gamma(D \to K^*\mu\nu)}{\Gamma(D \to K\mu\nu)}$ are presented in Table XII.

Table XII

Experiment	$\frac{\Gamma(D^+ \to \overline{K^{*0}}\mu\nu)}{\Gamma(D^+ \to K^-\pi^+\pi^+)}$	$\frac{\Gamma(D \to \overline{K^*}\ell\nu)}{\Gamma(D \to \overline{K}\ell\nu)}$
E691[23]	$0.49\pm0.04\pm0.05$	0.55 ± 0.14
E653 (μ)[24]	$0.46\pm0.07\pm0.08$	$0.43\pm0.09\pm0.09$
E687 (μ)[25]	$0.56\pm0.04\pm0.06$	$0.59\pm0.10\pm0.13$

There is a very good agreement between our results and the other experiments. As it is well known, there is a general discrepancy between these results and the expectations of the quark models.

The D decay to a vector particle introduces Lorentz invariant products of momenta and spins. Then the matrix element has to be written in terms of the three helicity amplitudes H_0, H_+ and H_- of the vector mesons:

$$\frac{d\Gamma}{dM_{K\pi}\cdot dt\cdot d\cos\vartheta_v\cdot d\cos\vartheta_\ell} = PS\times BW\times|M|^2$$

$$M = f\left[\cos\vartheta_\ell, \cos\vartheta_v, H_+(t), H_-(t), H_0(t)\right]$$

where: ϑ_v is the angle between π and D in the K^* frame; ϑ_e, between ℓ and D in the $\ell\nu$ r.f..

In the limit of massless leptons:

$$H_\pm = \alpha A_1(t)\pm\beta V(t)$$

$$H_0 = \delta A_1(t) - \varepsilon A_2(t)$$

$A_1(t)$ and $A_2(t)$ are the axial form factors; $V(t)$, the vector one. It is generally assumed that these form factors are given, in the one pole approximation, by: $F(t)=\frac{F(0)}{1-t/M_p^2}$, with the vector pole given by the D_s^* mass (~2.1 GeV) and the two axial poles given by the D_s^{**} mass (~2.5 GeV).

Adopting the E691 convention, the experimental measurements are concentrated on $R_V=\frac{V(0)}{A_1(0)}$ and $R_2=\frac{A_2(0)}{A_1(0)}$, which can be obtained by fitting the ϑ_v, ϑ_ℓ and t distributions.

The shape of the $\cos\vartheta_v$ intensity projection is controlled by the polarization parameter Γ_ℓ/Γ_t, e.i. the ratio of the longitudinal to transverse width of the virtual W:

$$\frac{d\Gamma}{d\Omega}\propto 1+(2\frac{\Gamma_\ell}{\Gamma_t}-1)\cos^2\vartheta_v,$$

The polarization parameter is a function of $|H_0|^2$ and $\left\{|H_+|^2+|H_-|^2\right\}$. R_v and R_2 are very crucially influenced by the systematic errors; then the systematic effects due to the MC statistics, detector efficiency variations and background are studied very carefully.

The E687 results are summarized in Table XIII. They agree very well with E653, while discrepancies exist with the E691 measurement of R_2 and Γ_ℓ/Γ_t. The confidence level for an agreement among the three experiments on R_2 and R_V is 60%.

Table XIII

Exp	R_2	R_v	Γ_l / Γ_t
E691	$0.0 \pm 0.5 \pm 0.2$	$2.0 \pm 0.6 \pm 0.3$	$1.8 ^{+0.6}_{-0.4} \pm 0.3$
E653	$0.82 ^{+0.22}_{-0.23} \pm 0.11$	$2.00 ^{+0.33}_{-0.32} \pm 0.16$	$1.18 \pm 0.18 \pm 0.08$
E687	$0.78 \pm 0.18 \pm 0.10$	$1.74 \pm 0.27 \pm 0.28$	$1.20 \pm 0.13 \pm 0.13$

The comparison of the results quoted in Table XIII with the theoretical predictions reveal, also in this case, a general disagreement between experiments and theory.

5.3 $D_s^+ \to \phi \mu^+ \nu$

We have selected a final yield of 123 ± 14 events. This signal was extracted by fitting the distributions of four kinematical variables, measured for the candidates, to a linear combination of the distributions predicted for the signal and six background sources, which are considered not negligible. The four variables are:

- $M(\phi\mu)$;
- the reconstructed proper time;
- $\cos\vartheta_v$, angle between the K^+ and the D_s direction in the ϕ r.f.;
- $\cos\vartheta_\mu$, angle between the ν and the D_s direction in the $\mu\ \nu$ r.f..

The BR with respect to the normalization channel $D_s^+ \to \phi\pi^+$ is shown in Table XIV.
The agreement of our results with CLEO and ARGUS is quite good.
The form factor measured with a procedure similar to the method used for $D^+ \to K^{*0}\mu^+\nu$, are:

$$R_v = 1.8 \pm 0.9 \pm 0.2; R_2 = 1.1 \pm 0.8 \pm 0.1.$$

The polarization parameter is $\Gamma_e / \Gamma_t = 1.0 \pm 0.5 \pm 0.1$

Table XIV

$\frac{\Gamma(D_s^+ \to \phi\mu\nu)}{\Gamma(D_s^+ \to \phi\pi^+)}$	
E687(μ)[25]	$0.58 \pm 0.17 \pm 0.07$
E691(e)[23]	<0.45
CLEO[22]	$0.49 \pm 0.10 ^{+0.10}_{-0.14}$
ARGUS[26]	$0.57 \pm 0.15 \pm 0.15$

6.0 Limits on C.P. violation

A good signature for CP violation is an asymmetry in the decay rate of a charm decay mode and its CP conjugate.

In order to produce such an asymmetry, we need two independent weak decay amplitudes, which contribute to the same final state (as Cabibbo suppressed decays or decay with mixing). In addition, final state interactions must induce a phase shift between the two decay amplitudes.

A good channel should be $D^0 \to K^-K^+$, which can be compared with $\overline{D^0} \to K^+K^-$. The charge of the D^* daughter π is used to divide the D^0 by the $\overline{D^0}$ sample. To measure the asymmetry we use the parameter:

$$A_{cp} = \frac{\eta(D) - \eta(\overline{D})}{\eta(D) + \eta(\overline{D})}$$

η is the $D, \overline{D}$ decay channel yield, normalized to a $D, \overline{D}$ Cabibbo allowed channel, as $\eta(D) = \frac{N(D^0 \to K^+K^-)}{N(D^0 \to K^-\pi^+)}$ and $\eta(\overline{D}) = \frac{N(\overline{D^0} \to K^-K^+)}{N(\overline{D^0} \to K^+\pi^-)}$. The normalization is needed to take into account the different D and $\overline{D}$ rates.

E687 has searched for CP violation, using the procedure described above[27]. The measured limits are: $|A_{CP}(K^+K^-)| < 13\%$[26] (90% Conf. Level).[previous limit <45%-E691[28]].

E687 studied also the decay channel $D^0 \to K^-K^+\pi^+$, by using $D^+ \to K^-\pi^+\pi^+$ as normalization channel. Here the situation is complicated by the possible intermediate resonant states. The CP asymmetry could be different for each decay mode, since the strong phase shift and the relative size of the two weak decay amplitudes vary. We studied the $K^{*0}K^+$ and $\phi\pi^+$ contributions, analysing the $K^\pm\pi^\mp$ and K^+K^- invariant mass distributions.

The measured limits (90% Conf. Level) are the following:

$A_{cp}(K^-K^+\pi^+)_{total} < 10\%$ $\quad A_{cp}(K^{*0}K) < 22\%$ $\quad A_{cp}(\phi\pi) < 12\%$

References

(1) P.L. Frabetti et al., Nucl. Instr. and Methods A320 (1992) 519
(2) P.L. Frabetti et al., Phys. Lett. B308 (1993) 193
(3) S. Frixione, M.L. Mangano, P. Nason and G. Ridolfi, Proc. of the Advanced Study Conference on "Heavy Flavours", Pavia, Sept. 1993, Ed. Frontieres; and private communication (paper in preparation)
(4) L. Rossi, private communication
(5) P.L. Frabetti et al., Phys. Rev. Lett. 71 (1993) 827
(6) P.L. Frabetti et al., Phys. Lett. B323 (1994) 459
(7) M. Bauer et al., Z. Phys. C34 (1987) 103
(8) H. Albrecht et al., Z. Phys. C46 (1990) 9
(9) J. Alexander et al., Phys. Rev. Lett. 65 (1990) 1184
(10) J.C. Anjos et al., Phys. Rev. D44 (1991) R3371
(11) M. Adamovich et al., Phys. Lett. B280 (1992) 163
(12) A. Kamal and S. Verma, Phys. Rev. D35 (1987) 3515
(13) A. Amstrong et al., Z. Phys. C, 51 (1991) 351
(14) J.C. Anjos et al., Phys. Rev. D43 (1991) R635
(15) H. Ammar et al., Phys. Rev. D44 (1991) 3383
(16) ARGUS Coll, preprint DESY 94-052
(17) P.L. Frabetti et al., Analysis of three $D \to K\pi\pi$ Dalitz plots - to be published in Phys. Lett. B
(18) H. Albrecht et al., Phys. Lett. B308 (1993) 435
(19) J.C. Anjos et al., Phys. Rev. D48 (1993) 56
(20) J.C. Anjos et al., Phys. Rev. Lett 60 (1988) 897
(21) Z. Bai et al., Phys. Rev. Lett. 66 (1991) 1011
(22) G. Crawford et al., Phys. Rev. D44 (1990) 3394; J.A. Alexander et al., Phys. Rev. Lett. 65 (1990) 1531
(23) J.C. Anjos et al., Phys. Rev. Lett. 65 (1990) 2630; Phys. Lett. 67 (1991) 1507; Phys. Rev.Lett. 64 (1990) 2885
(24) K. Kodama et al., Phys. Rev. Lett. 66 (1991) 1819; Phys. Lett. B286 (1992) 187; Phys. Lett. B274 (1992) 246
(25) P.L. Frabetti et al., Phys. Lett. B307 (1993) 262, Phys. Lett. B315 (1992) 203; Phys. Lett. B313 (1993) 253
(26) H. Albrecht et al., Phys. Lett. B255 (1991) 634
(27) P.L. Frabetti et al., Search for CP violation in charm meson decay, submitted to Phys. Rev. Lett.
(28) J.C. Anjos et al., Phys. Rev. 44 (1991) R3371
(29) A. Bean et al., Phys. Lett. B317 (1993) 647